Research

CrossMark
click for updates

THE ROYAL SOCIETY
PUBLISHING

Ab initio infrared vibrational modes for neutral and charged small fullerenes (C20, C24, C26, C28, C30 and C60)

Jean-Joseph Adjizian[1], Alexis Vlandas[2], Jeremy Rio[3], Jean-Christophe Charlier[1] and Chris P. Ewels[3]

[1]Institute of Condensed Matter and Nanosciences, Université Catholique de Louvain, Chemin des Étoiles 8, 1348 Louvain-la-Neuve, Belgium
[2]BioMEMS, Université Lille, CNRS, ISEN, UMR 8520-IEMN, 59000 Lille, France
[3]Institut des Materiaux Jean Rouxel, CNRS, University of Nantes, UMR6502, 2 Rue de la Houssiniere, BP32229, 44322 Nantes Cedex 3, France

J-JA, 0000-0002-7899-4565; AV, 0000-0003-2089-2360; J-CC, 0000-0002-5749-1328; CPW, 0000-0001-5530-9601

We calculate the infrared (IR) absorption spectra using DFT B3LYP(6–311G) for a range of small closed-cage fullerenes, C_n, $n = 20$, 24, 26, 28, 30 and 60, in both neutral and multiple positive and negative charge states. The results are of use, notably, for direct comparison with observed IR absorption in the interstellar medium. Frequencies fall typically into two ranges, with $C-C$ stretch modes around 1100–1500 cm^{-1} (6.7–9.1 µm) and fullerene-specific radial motion associated with under-coordinated carbon at pentagonal sites in the range 600–800 cm^{-1} (12.5–16.7 µm). Notably, negatively charged fullerenes show significantly stronger absorption intensities than neutral species. The results suggest that small cage fullerenes, and notably metallic endofullerenes, may be responsible for many of the unassigned interstellar IR spectral lines.

This article is part of the themed issue 'Fullerenes: past, present and future, celebrating the 30th anniversary of Buckminster Fullerene'.

1. Introduction

The recent confirmations of the presence of C_{60} and C_{70} in a wide range of interstellar and circumstellar

environments [1–6] have major implications for astrochemistry as well as the distribution of carbon in space. These results have been contingent on two factors: the high-quality infrared (IR) results provided by the Spitzer telescope infrared spectrograph instrument [7] and the knowledge gained by theoretical and experimental studies on the IR signatures of these fullerenes [8–12]. In addition to detection in their neutral state, fullerenes have been found to be prevalent in space in charged states. In fact, owing to their low ionization potential, it was foreseen in the late 1980s [13] that C_{60} could easily be stripped of an electron to become C_{60}^+, at least in the gas phase. This charged fullerene has recently been confirmed to be the origin of two diffuse interstellar bands [14] and was evaluated to represent up to 0.9% of interstellar carbon [15]. Cationic fullerenes may also exist in space, notably via charge transfer from endohedral metal atoms trapped within the fullerene cage [16]. Dunk *et al.* [8] have recently proposed that the $Na@C_{60}$ metallic endofullerene provides a mechanism for ^{22}Na capture during supernova events, and subsequent incorporation of its decay product ^{22}Ne in carbonaceaous dust in the interstellar medium.

Notwithstanding the advances made in detecting the contribution of fullerenes to the IR spectra of various stellar objects, the attribution to specific species of the remaining observable spectral features is an ongoing process. A major effort has been made to collect experimental and theoretical spectra for polycyclic aromatic hydrocarbons (PAHs) [17]. The confirmation of the existence of stable small closed-caged fullerenes [18,19] and endohedral metallofullerenes [20] extends the range of candidates for this process. These fullerenes have specificities that differ from those of their larger cousins that need to be taken into account. They display interesting motifs in their structure such as squares and paired or triple pentagons, and their synthesis is likely to be metal assisted [21]. However, until such species can be chemically isolated and their individual IR spectra measured, direct assignment to stellar IR spectral lines remains elusive.

For this reason, this paper presents calculated IR absorption spectra for the smallest closed-cage fullerenes of C_n, where $n = 20, 24, 26, 28$ and 30, as well as of C_{60} for comparison. We do so in both neutral and various positive and negative charge states. The positive charge state calculations are important because, as discussed above for C_{60}, under strong 13.6 eV irradiation in diffuse interstellar space, electron loss is likely and hence observed fullerenes are likely to be positively charged.

We include the negatively charged fullerene results for comparison with metallic endofullerenes [22]. For C_{60}, it was noted that $Na@C_{60}$ and C_{60}^- IR spectra are effectively identical [8]. This is coherent with the ionic metal–fullerene bonding model whereby charge is transferred from the metal to the fullerene and is not highly localized. This phenomenon has been investigated by Kobayashi and co-workers [23,24] and shown to be the norm (with the exception of the $Sc_3N@C_{78}^{n-}$ system, which shows covalent characteristics). Experimentally, the vibrational spectra of $M@C_{82}$ (Y, La, Ce, Gd) in the IR range were measured by Lebedkin *et al.* [25]. The spectra were found to be virtually identical in the range above $200\,cm^{-1}$, consistent with a picture whereby the role of the endohedral metal is primarily one of charge transfer to the surrounding cage, with little or no other perturbation of the cage itself. We therefore hypothesize that in the case of small closed-cage fullerenes one can determine the likely IR spectra for endohedral metal fullerenes by simply negatively charging the empty fullerene cage appropriately.

2. Material and methods

Calculations were performed with density functional theory (DFT) as implemented in the Gaussian09 code [26] using B3LYP exchange correlation and a 6–311G basis set, following the method tested and successfully applied to C_{60} and $Na@C_{60}$, both in a range of charge states [8]. In that paper [8], we compared the 6–31G* and 6–311G basis sets, finding a better match to experimental IR spectra for the larger 6–311G basis without the need for a frequency scaling factor. We note that the NASA AMES PAH database [17] uses a 4–31G basis set to calculate IR signatures of PAHs [27]. For comparison, we also calculated the IR spectra for C_{20} and C_{60} in various charge states with this basis set, obtaining near identical results to the 6–311G basis (see the electronic supplementary material, figure S1). In their comparative analysis to experimental

Table 1. Small cage fullerenes considered in this study, including their symmetry group in the neutral charge state and thermodynamically most stable spin multiplicities. C_{60} is included for comparison.

|	symmetry	stable multiplicity for given charge state								
		+4	+3	+2	+1	0	−1	−2	−3	−4
C_{20}	I_h	3	2	1	2	1	4	1	2	1
C_{24}	D_{6d}	1	2	3	2	1	2	1	2	1
C_{26}	D_{3h}	3	2	5	6	5	4	3	2	1
	C_s	1	2	1	4	3	2	1	2	1
C_{28}	T_d	1	2	3	4	5	4	3	2	1
	D_2	3	2	1	2	1	2	1	2	1
C_{30}	C_{2v}–I	5	4	3	2	1	2	1	2	1
	C_{2v}–II	3	2	1	2	3	2	1	2	1
C_{60}	I_h	3	4	3	2	1	2	3	4	3

spectra, they apply a constant $15\,\mathrm{cm}^{-1}$ red shift to their calculated values [17] and a 0.986 scaling factor to all modes [27].

For each fullerene and for charge states ranging from -4 to $+4$, the structures are fully relaxed using a conjugate gradient algorithm or a quadratically convergent self-consistent field procedure ('XQC optimization') when the conjugate gradient failed, and normal frequencies are then calculated. Different multiplicities ranging from singlet to quintet have been checked and the most stable is reported (table 1). Calculations are carried out until forces on each atom are less than $0.04\,\mathrm{eV\,\mathring{A}}^{-1}$. In the calculations, the force constants are determined analytically and the vibrational frequencies are computed by determining the second derivatives of the energy with respect to the Cartesian nuclear coordinates. Spectra are generated using Gaussian broadening with $15\,\mathrm{cm}^{-1}$ full-width at half-maximum (FWHM) for frequency spectra and $0.25\,\mu\mathrm{m}$ FWHM for wavelength plots. Different charge states have intensities offset on the IR plots by $40\,\mathrm{km\,mol}^{-1}$ for improved visibility. The plots given in the paper show frequency on the x-axis; equivalent plots with wavelength on the x-axis are included in the electronic supplementary material. All vibrational frequencies are positive, confirming that the optimization has reached a minimum energy structure.

3. Results

After initially considering C_{60}, we present each of C_{20}, C_{24}, C_{26}, C_{28} and C_{30} in sequence. Considering classical fullerene pentagon–hexagon structures, there are only a limited number of isomers for these small size fullerenes; indeed, C_{20}, C_{24} and C_{26} have only one available isomer, there are two isomers for C_{28} (T_d and D_2 symmetry), and three for C_{30}. We have excluded the D_{5h} isomer of C_{30} from this study because it is significantly less thermodynamically stable than the other two. In addition to these species, we have also included a C_s symmetry isomer of C_{26} constructed from a square, 10 pentagons and 3 hexagons. Fullerenes containing square motifs have been proposed as more stable isomers for small fullerenes [28] because they are able to localize curvature more effectively and hence relieve surface strain elsewhere in the fullerene cage. As they should also have distinct IR signatures associated with distorted square motifs, we felt this was valuable to include.

We note that, for the pentagon–hexagon isomers, the relative energy of the anions and cations between different isomers matches that of the neutral species, validating the ionic model
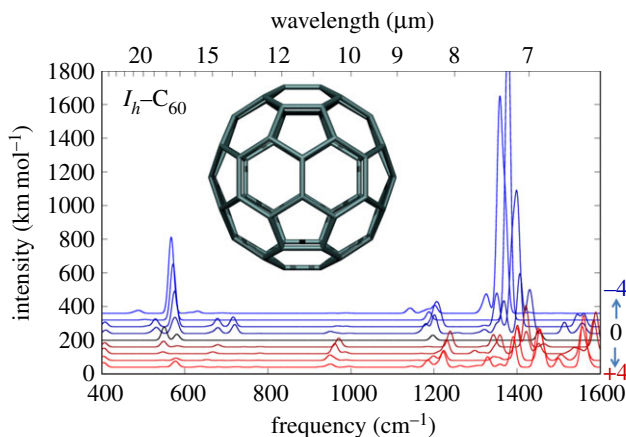
Figure 1. Calculated IR spectra in cm^{-1} for I_h-C_{60} in various charge states. (Online version in colour.)

discussed above. This is also the case for the non-classical $C_s - C_{26}$ square-containing isomer, which we find less stable than its conventional D_{3h} isomer in all charge states, in agreement with the results of An *et al.* [29].

(a) C_{60}

The IR absorptions associated with C_{60}, and its charged species C_{60}^+ and C_{60}^-, have been extensively explored in the literature [8–12] and serve as a useful benchmark for our calculations. C_{60} has only four vibrational IR absorption lines due to its I_h symmetry, at 1436, 1191, 574 and 531 cm^{-1} in the 0 K gas phase [9,10]. Removal of an electron gives C_{60}^+, the electronic transitions of which were recently identified as the source of two strong diffuse interstellar bands at 9632.7 Å and 9577.5 Å [14] and weaker bands at 9428.5 Å and 9365.9 Å [30]. Charging the fullerene breaks its symmetry, giving rise to extensive new IR active vibrational modes [31], notably a high-frequency mode at approximately 1550 cm^{-1} (6.45 μm) due to vibrations of pentagons at opposing ends of the fullerene cage [8]. The IR bands possibly due to C_{60}^+ have been tentatively assigned in spectra from objects Tc1, SMP SMC 16, NGC 7023, NGC 2244 and SMP LMC 02, while features possibly due to C_{60}^{2+} were identified in NGC 7023 [32].

Our calculated frequencies for neutral C_{60} lie at 1453.5 cm^{-1}, 1197.2 cm^{-1}, 580.8 cm^{-1} and 550 cm^{-1}, in good agreement with experiment (figure 1). In C_{60}^+, the symmetry is broken and many more modes are visible; notably, we see strong peaks in the calculations at 1584, 1542, 1467, 1434, 1360, 1314, 1231, 1187, 965 (726 and 686) and 549 cm^{-1}, agreeing with experimental measurements of C_{60}^+ in a Ne matrix [31], with the exception of our peak at 1434 cm^{-1} not reported in the experiment, presumably because of its overlap with neutral C_{60} at 1432 cm^{-1}. C_{60}^{2+} was also measured in a Ne matrix [33], and again we have excellent agreement on all peak positions with the exception of peaks around 1450 cm^{-1}, which again may be due to C_{60} signal masking. C_{60}^- shows excellent peak-to-peak matching with experimental data in the Ne matrix [31], with the calculated (experimental) peaks as follows: 1563 (1546), 1450 (*), 1410 (1386), 1349 (1352), 1320 (1334), 1206 (1201), 1194 (1176), 974 (964), 727 (729), 681 (*), 576 (576 and 575), 542 (*) and 401 (397) cm^{-1}; asterisks indicate no experimental peak (in the case of 1450 cm^{-1} and 542 cm^{-1}, once again probably due to neutral C_{60} masking). The strongest peak is at 1410 cm^{-1}.

We note that the total energies are very close to each other between the doublet/quartet and the singlet/triplet (approx. 1 meV) spectra for C_{60}^{3-} and C_{60}^{4-}, respectively, with those of the triplet/quartet being the most stable. The strong peak at approximately 1580 cm^{-1} discussed above is present in the calculated singlet/doublet spectra for C_{60}^{3-} and C_{60}^{4-}, but not for the triplet/quartet systems.
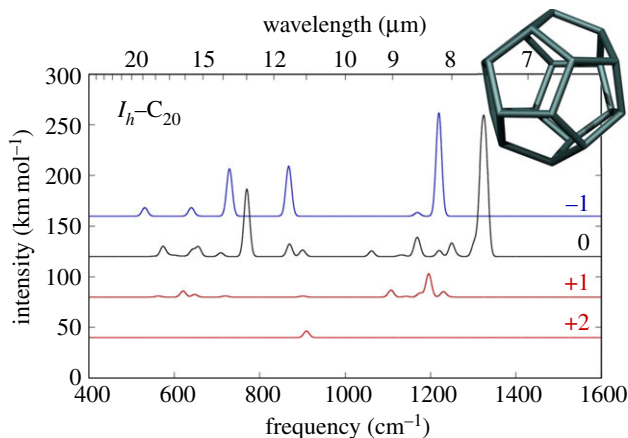
Figure 2. Calculated IR spectra for I_h–C_{20} in cm^{-1} in various charge states, as marked. (Online version in colour.)

It is important to note that our calculated IR intensities for C_{60}^- are over an order of magnitude higher than those for C_{60}. In general, the peak intensities are significantly higher for the negatively charged than for the neutral fullerene species considered here. This trend is consistent with the observed higher peak intensities in IR for metallic endofullerenes when compared with their equivalent empty cage spectra [8,16,34,35]. This suggests that metallic endofullerenes may be disproportionately represented in experimental IR spectra.

The excellent agreement between literature experimental values for C_{60} in a range of different charge states and the calculated theoretical values presented here gives us confidence in the calculated frequencies presented below. We note that a scaling factor of approximately 0.99 in general brings all the modes even closer to experiment, independent of the fullerene charge state. Thus while no scaling factors are applied throughout this article, this factor may be useful for future spectral line identification.

(b) C_{20}, the smallest cage

Experimentally the monocyclic isomer of C_{20} dominates and there is no experimental evidence for direct C_{20} fullerene formation [20], although it can be (briefly) synthesized by gas-phase removal of the functional groups from $C_{20}H_{20}$ [36]. However, we include it here as the smallest possible classical fullerene cage, for comparison with previous literature calculations, and because of its structural motif consisting of purely fused pentagons, which should result in a distinctive IR signature. Although the perfect cage shows icosahedral I_h symmetry, it has been shown that the structure can relax through a Jahn–Teller distortion to a D_{3d} structure [37]).

The calculated spectrum for neutral C_{20} (figure 2) agrees well with previous literature data (B3LYP with the 6–31++G basis [38] and 6–31G(d) basis [39]), featuring two primary peaks at 1324 cm^{-1} (7.55 μm) and 769 cm^{-1} (13.00 μm). Peaks in these two spectral regions are seen in many of the small fullerene spectra discussed below. The peak at 1324 cm^{-1} corresponds to tangential carbon–carbon bond stretching (figure 3), at lower frequency than the C–C stretch mode in C_{60} or graphene due to the longer, weaker bonds in C_{20}. The peak at 769 cm^{-1} is fullerene cage specific and involves radial motion of the carbon atoms. Opposing pentagon corners move radially in phase, while the remaining carbon atoms move radially with alternating phase. The result is a synchronized torsional motion around the central circumference of the fullerene. The symmetric radial breathing mode where all atoms move radially towards the fullerene centre is IR inactive, and is calculated at 816 cm^{-1} (12.25 μm). C_{20}^+ loses the strong peak at 769 cm^{-1}, while the 1324 cm^{-1} peak is split into multiple peaks, with the primary feature at 1195 cm^{-1} (8.37 μm). Signal intensity is significantly weaker than for the neutral, and for C_{20}^{2+} the signal intensity is nearly two orders of magnitude weaker than for the neutral species. There is a general tendency

(a) (b)
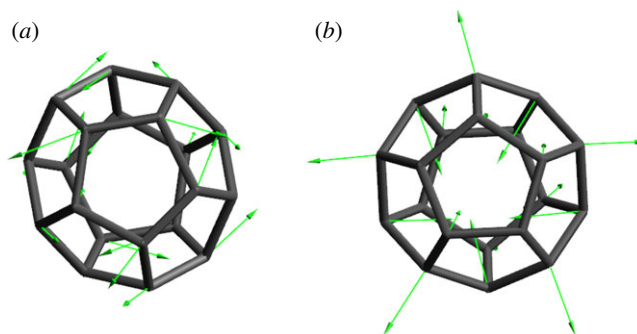
Figure 3. Calculated eigenvectors for neutral I_h–C_{20} modes at (a) 1324 cm^{-1} (7.55 μm), primarily associated with carbon–carbon stretch, and (b) 769 cm^{-1} (13.00 μm), involving coupled torsional motion of the fullerene cage circumference. (Online version in colour.)
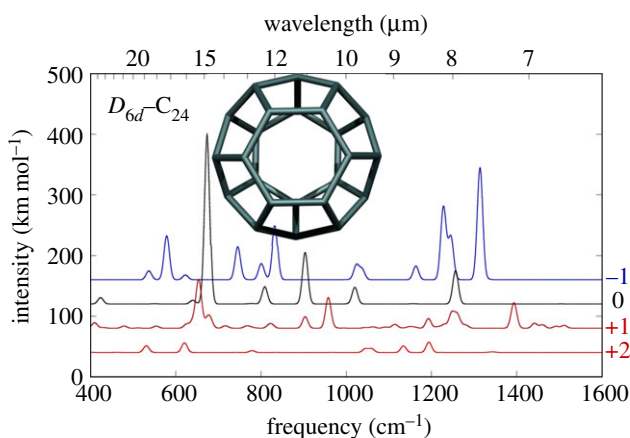
Figure 4. Calculated IR spectra for D_{6d}–C_{24} (cm^{-1}) in various charge states, as marked. (Online version in colour.)

of downshifting frequency (increasing wavelength) of the peaks with increasing negative charge on the cage.

## (c) C_{24}, the transition from rings to fullerenes

C_{24} is close to the thermodynamic transition between stable ring and fullerene structures [1–6,40,41], and under certain experimental conditions can be a stable product from carbon vapour condensation [42]. There is only one classical fullerene isomer of C_{24}, the highly symmetric D_{6d} form consisting of an opposing hexagon pair connected by two rings of six pentagons each (figure 4), although calculations suggest that a non-classical isomer incorporating two squares may be energetically competitive [28]. It is suggested that the D_{6d} symmetry can be lifted through a small Jahn–Teller distortion to D_6 [37].

The high fullerene symmetry results in a dominating peak for the neutral species at 674 cm^{-1} (14.84 μm), with secondary peaks at 903 and 1255 cm^{-1} (11.07 and 7.97 μm), again in good agreement with literature calculations (DFT-PBEPBE/6–31G(d,p) [43]) (figure 4). The 674 cm^{-1} peak has a similar character to the 769 cm^{-1} mode described above for C_{20}, i.e. a coupled torsional mode around the equator of the fullerene, with in-phase motion of the capping hexagons (figure 5). Positive charging leads to a rapid decrease in IR intensities with slight shifting of all features.
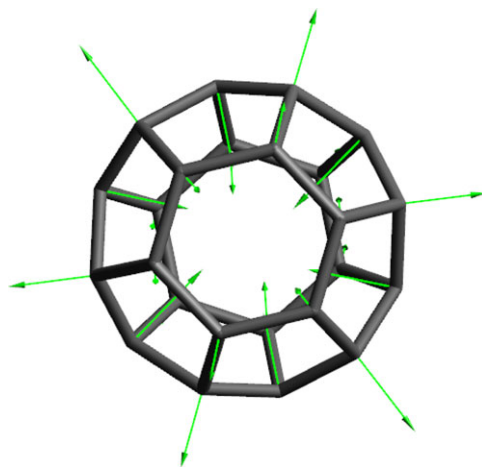
Figure 5. Calculated eigenvectors associated with the 674 cm^{-1} (14.84 μm) mode of neutral D_{6d}–C_{24}. (Online version in colour.)
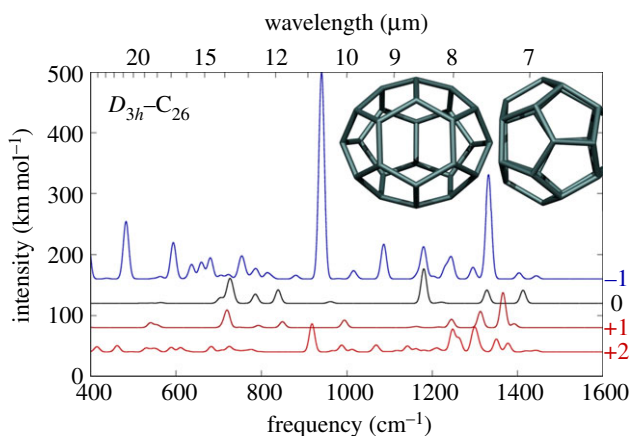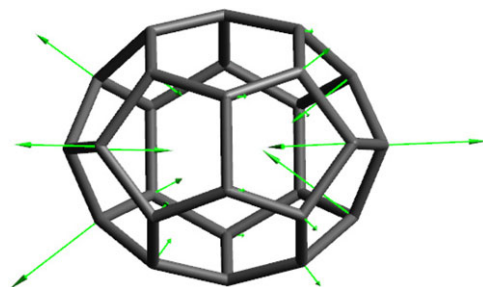

Figure 6. Calculated IR spectra for D_{3h}–C_{26} (cm^{-1}) in various charge states, as marked. (Online version in colour.)

(d) C_{26}, exploring square motifs

The next closed fullerene cage by size is C_{26}, of which there is only one classical closed-cage isomer, with D_{3h} symmetry. The cage consists of opposing triply fused pentagons, bridged by a ring of three alternating hexagon and pentagon pairs. However there are other non-classical isomers, and we also consider here a C_s – C_{26} isomer containing a single square that was found to be close in energy to the classical cage [29]. The square replaces two pentagons, and the structure also contains four hexagons, three of which are localized around the square. Both of these structures are the first we have considered with an open shell electronic structure in the neutral charge state (quintet and triplet, respectively), with the classical isomer being 5.29 kcal mol^{-1} more stable.

There is once again good agreement with an available literature spectrum for the neutral species (B3LYP/6–31G* basis) [29] (figure 6), with primary peaks at 1180 and 726 cm^{-1} (8.47 and 13.77 μm), and secondary peaks at 1413, 1328 and 839 cm^{-1}. The 1180 cm^{-1} peak corresponds to pentagon–pentagon C−C stretch. The 726 cm^{-1} peak corresponds to the two triplet pentagons at opposing ends of the cage, with the apex carbon atoms vibrating in phase along the fullerene axis, while their three surrounding neighbours vibrate radially out of phase with the apex atoms

Figure 7. Calculated eigenvectors associated with the 726 cm^{-1} (13.77 μm) mode of neutral D_{6d}–C_{24}. (Online version in colour.)
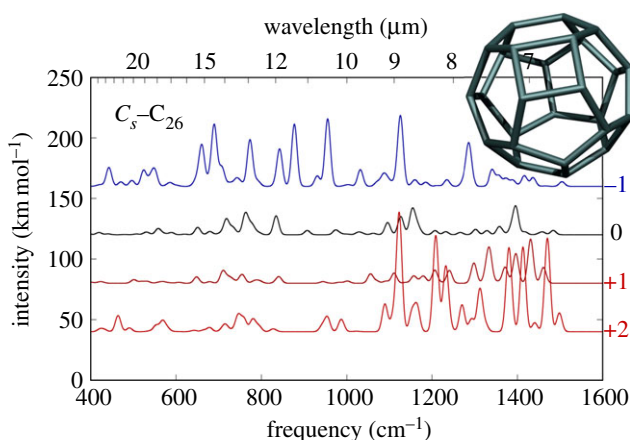
Figure 8. Calculated IR spectra for C_s–C_{26} (cm^{-1}) in various charge states, as marked. (Online version in colour.)

(figure 7). Thus, this mode is distinctly characteristic of triplet-pentagon groups. All primary peaks in the 600–750 cm^{-1} range discussed thus far share the common feature of radial carbon motion at the centre of triple pentagons.

The stable spin state for the neutral species is the quintet (multiplicity of 5), and the calculated IR spectrum shows qualitative differences if the electrons are spin-flipped. Notably, the singlet structure, 10.91 kcal mol^{-1} less stable than the quintet, shows a primary peak at approximately 1080 cm^{-1} instead of 1180 cm^{-1} for the quintet.

The C_s − C_{26} isomer does not have such strongly defined IR peaks (figure 8). It is difficult to clearly identify specific peaks with the square motif as all modes are coupled around the cage. Nonetheless, the C−C stretch mode of the square is strongly active in the mode at 973 cm^{-1}, while the peak at 620 cm^{-1} demonstrates a similar radial carbon motion as described previously for triplet pentagons, but in this case for a carbon atom forming part of the square. The cage has an IR inactive radial breathing mode at 706 cm^{-1}.

(e) C$_{28}$, the beginning of metal encapsulation

C$_{28}$ is the first of the 'magic number' fullerenes and, arguably, the most important of those considered in this study. The most stable classical isomer, T_d–C_{28} is the smallest fullerene to contain isolated triple-pentagon groups, one at each corner of its tetrahedral cage structure. This results in highly localized curvature, stabilizing the fullerene sides and rendering the corners highly chemically reactive, as the central carbon atom of each pentagon triplet is essentially a sp^3-coordinated dangling bond. The structure can be chemically stabilized by hydrogenating these
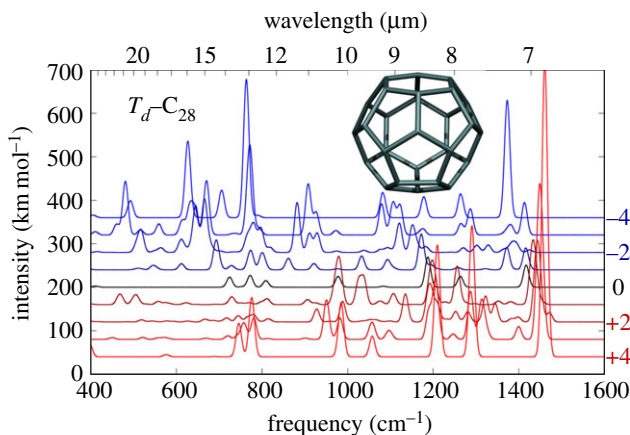
Figure 9. Calculated IR spectra for T_d–C_{28} (cm^{-1}) in various charge states, as marked. (Online version in colour.)

dangling bonds to give $C_{28}H_4$ [44], forming a closed shell species, or through charge transfer, giving C_{28}^{4-}, typically through encapsulation of a 4+ metal cation.

This unique structure means that C_{28} is the smallest fullerene cage for which metal encapsulation has been demonstrated experimentally [20]. The first metal-encapsulated C_{28} species to be detected was U@C_{28} [45], relatively early in the history of fullerene research, and more recently Ti@C_{28}, Zr@C_{28}, U@C_{28} and even Hf@C_{28} have been unambiguously identified [20]. For larger metal species, the internal cavity of C_{28} remains too small for encapsulation, for example the smallest Th-encapsulated cage is Th@C_{36} [20], and similarly the La metal in LaC_n^+ fullerene species was shown to be exohedral for $29 < n < 35$, and only endohedral for $36 < n < 90$ [46]. Thus with the possibility of endohedral metal doping, for the purposes of our calculations, C_{28} is the first cage species for which it becomes important to determine the IR spectra at potentially high charge states up to C_{28}^{4-}.

C_{28} is a common product from laser vaporization of C_{60}, suggesting that if C_{60} is present in large quantities in interstellar environments, under irradiation, C_{28} may also be expected to exist. Equally, $C_{28}H_4$ is highly stable, for example field-evaporated graphite also results in a strong $C_{28}H_4^+$ signal [47]; subsequently hydrogen loss may also lead to the C_{28} presence in space.

For neutral T_d–C_{28}, there are two primary modes at 1417 and 1188 cm^{-1}, with weaker modes at 1263, 978, 772, 724 and 809 cm^{-1} (figure 9). However, this picture changes significantly upon charging to C_{28}^{4-}. Firstly, signal intensity increases by a factor of nearly five and the primary peaks now lie at 763 cm^{-1} and 1373 cm^{-1} (13.11 and 7.28 μm), with a secondary peak at 625 cm^{-1} (16.0 μm) and weak peaks (absorption comparable to the neutral species) at 492, 705, 1082, 1178 and 1264 cm^{-1}. The C_{28}^{3-} charge state similarly has a primary absorption feature at 771 cm^{-1} (12.97 μm) with intensity approaching that of the C_{28}^{4-} peaks, and weaker peaks at 908, 670 and 480 cm^{-1}. The 763 cm^{-1} triplet mode for C_{28}^{4-} comes from radial breathing of a triple-pentagon carbon atom and its surrounding 10 neighbours, in phase with a radial motion of a hexagon on the opposing side of the cage. The 1373 cm^{-1} triplet mode comes from hexagon C−C bond stretching (figure 10).

Comparing our C_{28}^{4-} result with previous calculations for Ti@C_{28} shows qualitatively good agreement [48], with strong peaks for Ti@C_{28} reported at 1357/1396 cm^{-1}, and several bands around 780–830 cm^{-1}. This peak splitting compared with our results comes from symmetry breaking by the Ti atom, which displaces from the cage centre towards one of the triplet-pentagon centred carbon atoms. This suggests limitations to the ionic metal–fullerene bonding model for small fullerenes where hybridization with the encapsulated metal atom also takes place.

For completion, we also include here the second classical C_{28} fullerene isomer, D_2–C_{28}. This isomer has six pentagons at each fullerene end, linked via four hexagons around the fullerene
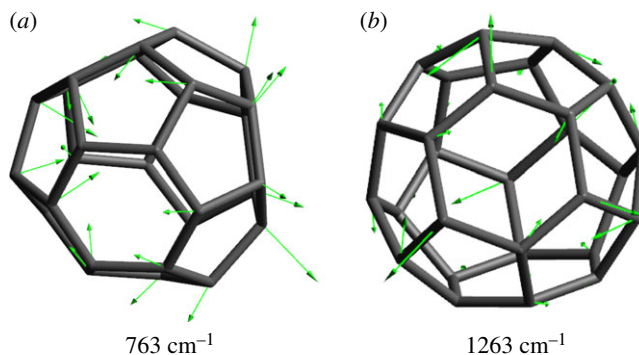
Figure 10. Calculated eigenvectors associated with the (a) 763 cm^{-1} (13.11 μm) and (b) 1263 cm^{-1} (7.28 μm) mode of neutral T_d–C$_{28}$. (Online version in colour.)
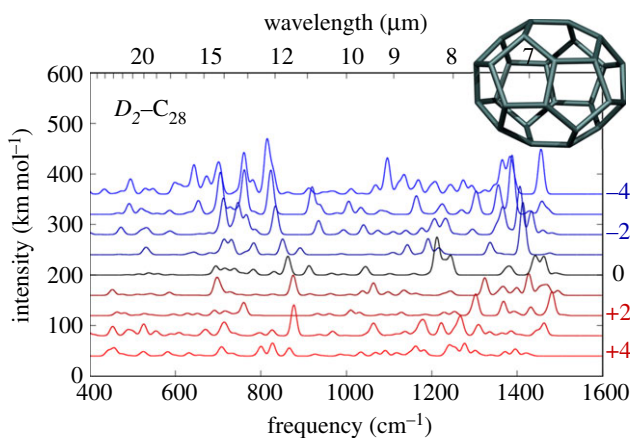
Figure 11. Calculated IR spectra for D_2–C$_{28}$ (cm^{-1}) in various charge states, as marked. (Online version in colour.)

equator. As it is 30.84 kcal mol^{-1} less stable than T_d–C$_{28}$, it is unlikely to exist in significant quantities. As for the previous species discussed, D_2–C$_{28}$ exhibits strong absorption in the 700–800 and 1200–1500 cm^{-1} regions with precise peak positions depending on the charge state (figure 11). Again in common with previous species, IR absorption intensity is significantly higher for the negatively charged fullerenes. The primary neutral D_2–C$_{28}$ modes at 863 and 1212 cm^{-1} (11.59 and 8.25 μm) correspond similarly to radial and bond stretch (tangential) carbon motion, respectively.

(f) C$_{30}$

There are three classical isomers of C$_{30}$. We find that the ground state C_{2v}–II–C$_{30}$ isomer is 6.23 kcal mol^{-1} more stable than C_{2v}–I–C$_{30}$, which is in turn 52.98 kcal mol^{-1} more stable than D_{5h}–C$_{30}$. Owing to the low stability of this third isomer, we consider only the two C_{2v} species here. While C$_{30}$ is experimentally much less common than C$_{28}$ and not a 'magic number' fullerene, it is nonetheless detected in laser ablation studies, and the metallic endofullerene Ti@C$_{30}$ has been observed, albeit in lower concentrations than Ti@C$_{28}$ [20]. Thus, we include it here for completion but do not expect it to be a major source of interstellar carbon.

The spectra of C_{2v}–II–C$_{30}$ nicely follow the general trend seen above with peaks in two primary spectral windows (figure 12b). The first group of peaks lie in the 1100–1500 cm^{-1} range, peaking at 1217 cm^{-1} (8.22 μm) for the neutral species and increasing in frequency and intensity with increasing charge state to 1434 cm^{-1} (6.97 μm) for C_{2v}–II–C$_{30}^{4-}$. Strong absorptions are also seen

at approximately 700–800 cm^{-1}, the most intense at 776 cm^{-1} (12.89 μm) for C_{2v}–II–C_{30}^{4-}, notably increasing in strength with negative charging and spreading to lower frequencies. The spectra for C_{2v}–I–C_{30} also show the same general trend (figure 12a).

4. Discussion and conclusion

In order to draw some general conclusions, in figure 13 we show the calculated IR spectra for all of the neutral charge state fullerenes considered here, versus frequency (cm^{-1}) and wavelength (μm). Certain common features can be observed. In general, the IR absorption bands fall into two broad spectral regions: the first in the approximately 1200–1400 cm^{-1} range (approx. 6–8.5 μm), the second in the approximately 700–800 cm^{-1} range (approx. 12–14.5 μm), with a few additional peaks at other frequencies. The first of these ranges correspond to C−C stretch modes, tangential to the fullerene cage surface, and overlap with vibrational modes of most sp^2-carbon-based molecules. The second range however corresponds to radial motion of carbon atoms involved with shared pentagons, and can be considered 'fullerene specific'. Peaks in this second range are notably more intense when they involve carbon atoms at the centre of triple-pentagon patches. These peaks can be understood because carbon atoms shared between pentagons are chemically under-coordinated and have dilated C−C bonds as a result, explaining why this mode is not present in isolated pentagon fullerenes C_{60} and above.

A second general observation is that calculated IR intensities are generally much higher (up to an order of magnitude) for strongly charged fullerenes, notably negatively charged. This is particularly true for T_d–C_{28} and I_h–C_{60}. In general, this can be understood through the increased dipole moment associated with vibrating charged cages. Additionally, the IR intensity is enhanced in cases with a carbon radical (dangling bond) at the centre of triple pentagons. In these cases, excess negative charge localizes on these sites, for example in $T_d − C_{28}^{4-}$ the Mulliken charge on these four symmetric corner atoms is 0.331e/C with 0.179e/C on the 12 neighbouring sites. By comparison, in C_{60}^- the charge is distributed evenly over the cage (with some symmetry breaking), ranging from 0.004e to 0.033 e/C. This charge localization means that radial vibrations associated with these sites, such as the approximately 700 cm^{-1} mode seen in many of the negatively charged cages examined here, have significantly stronger dipole moment and thus IR absorption. Our negatively charged cage results show generally good agreement with the previous calculations of metallic endofullerenes that were available, suggesting that they can be used as good indicators of spectral features of metallic endofullerenes. We note that the enhanced intensity for strongly charged species suggests that metallic endofullerenes will show disproportionately strong interstellar absorptions relative to their concentrations.

These closed-cage small fullerenes and their metallic endofullerene equivalents may be stable enough to be found in interstellar space, and it is our hope that the current calculated spectra can now be linked to interstellar spectral data. Figure 14 shows Spitzer data from planetary nebula of the Magellanic cloud, which have been investigated for the presence of C_{60} and C_{70}. These are residual spectra, adapted from García-Hernández et al. [49], for which the dust continuum emission has been subtracted. We have indicated the position of the peaks obtained from our calculations as vertical lines. Figure 14a includes our 20 strongest calculated lines from neutral and +1 species, and figure 14b includes those from the negatively charged species, which we take as indicative of potential endohedral metallofullerene absorptions (values listed in table 2).

We emphasize that the exact position of these lines is strongly influenced by the scaling factor chosen to account for inaccuracies in the calculation and thermal effects. This is particularly true for the long wavelength modes where the use of a single scaling constant for all systems is far from ideal. For this study, we have chosen to align our data on the 19.011 μm C_{60} peak, but these figures should only be taken as qualitative indicators of potential peak positions and do not have sufficient accuracy for quantitative peak assignment. Future calculations could make use of significantly larger basis sets to improve this. Equally, we emphasize that for clarity we have plotted only the 20 strongest lines in each case.

12

rsta.royalsocietypublishing.org   Phil. Trans. R. Soc. A 374: 20150323
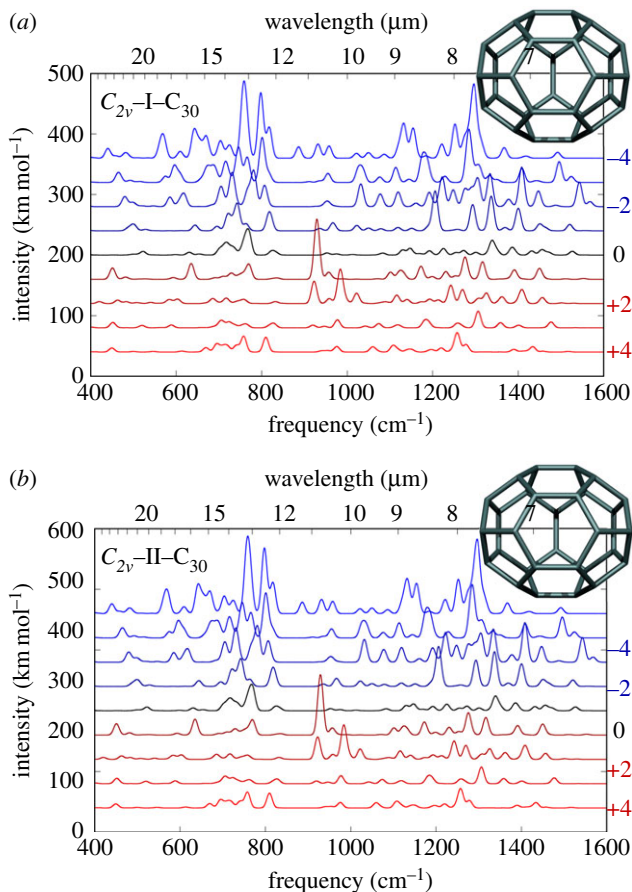
Figure 12. Two principal classical fullerene isomers of C_{30}: (a) C_{2v}–I–C_{30} and (b) C_{2v}–II–C_{30}. Isomer structures and calculated IR spectra in cm^{-1} in various charge states, as marked. (Online version in colour.)
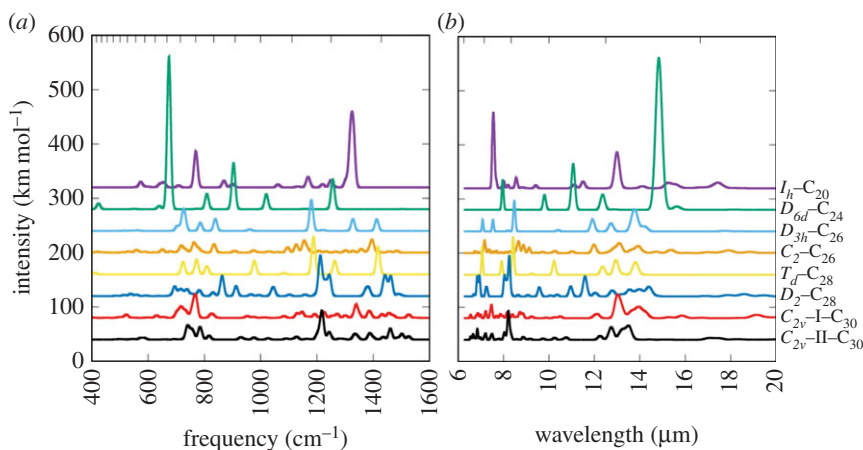
Figure 13. Calculated IR spectra in (a) cm^{-1} and (b) μm for small fullerene cages C_n, $n = 20$–30, and C_{60}, all in the neutral charge state. (Online version in colour.)
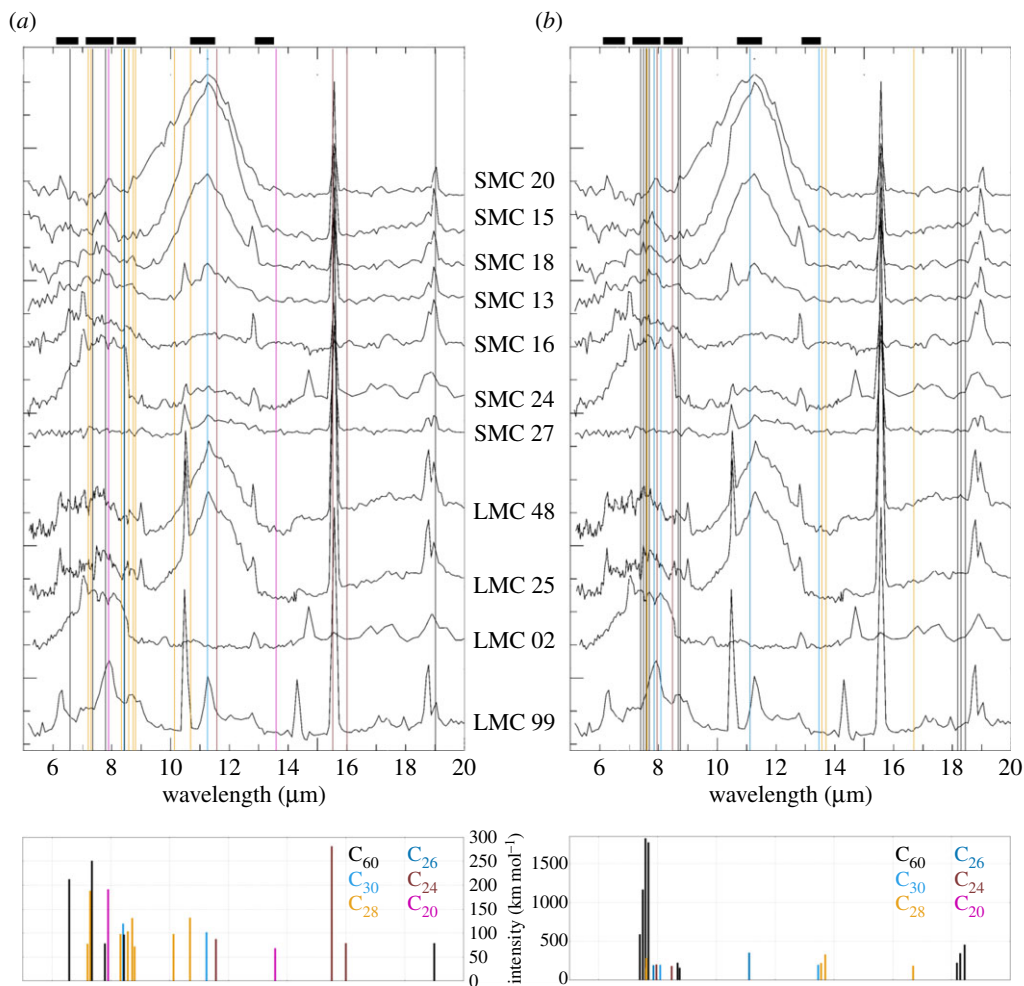
Figure 14. Experimental residual spectra from Spitzer measurements of planetary nebula in the Magellanic cloud with dust continuum emission subtracted (Adapted from García-Hernandez *et al.* [49].) Overlaid are lines showing the 20 most intense calculated IR absorption modes for C_{20}–C_{30} and C_{60}, colour coded based on the fullerene, wavelengths scaled to align the C_{60}^0 mode at 19.011 μm. (*a*) Neutral and +1 charged fullerenes; (*b*) −1, −2, −3 and −4 charged fullerenes (indicative of metallic endofullerenes). Impulses plotted below show the intensities of each calculated mode. The black bars above each spectrum mark the spectral ranges with calculated absorption by PAHs summed from the NASA AMES PAH database [27] (see the electronic supplementary material, figure S13). Calculated values are listed in table 2.

The black bands at the top of each plot indicate the main features from 490 summed PAH species from the NASA AMES theoretical PAH database (electronic supplementary material, figure S13). As can be seen, one of the major challenges, which might reduce detection chances, is the spectral overlap between these fullerene cages and the PAHs. Notably, they strongly overlap in the IR stretching mode region around 6–8.5 μm, making unique assignment difficult. Interstellar bands are reported at 3.3, 6.2, 7.7, 8.6, 11.2 and 12.7 μm (and weaker ones at 13.5 and 14.1 μm) and features seen at these energies are commonly identified as PAHs, although there has not yet been a conclusive identification of the carrier(s) [50–52]. More recently, effort has been devoted to analysing 15–20 μm features corresponding to C−C−C modes [53]. These modes, often (but not always) 10 times weaker in most stellar regions, are centred at around 15.8, 16.4, 17.4, 17.8 and 18.9 μm. We therefore suggest that a promising strategy to assign closed-cage

Table 2. The 20 most intense IR absorption modes from all calculated fullerenes in the paper for the (left) neutral and $+1$ species and (right) -1 to -4 charged species (as plotted in figure 14). Values taken from the Gaussian broadened data, with a 1.046 scaling factor applied to align on the experimental 19.011 µm C_{60}^0 peak.

neutral, $+1$ species					$-1, -2, -3, -4$ species				
fullerene	charge	wavelength (µm)	frequency (cm^{-1})	intensity (km mol^{-1})	fullerene	charge	wavelength (µm)	frequency (cm^{-1})	intensity (km mol^{-1})
$D_{6d}-C_{24}$	0	15.52	644.1	279	I_h-C_{60}	-3	7.59	1316.9	1815
I_h-C_{60}	$+1$	7.36	1358.6	249	I_h-C_{60}	-4	7.69	1301.1	1761
I_h-C_{60}	$+1$	6.59	1518.5	211	I_h-C_{60}	-2	7.50	1333.1	1154
I_h-C_{20}	0	7.91	1264.9	189	I_h-C_{60}	-1	7.40	1352.1	578
T_d-C_{28}	$+1$	7.30	1370.7	186	I_h-C_{60}	-4	18.45	542.1	442
T_d-C_{28}	$+1$	10.69	935.1	130	$D_{3h}-C_{26}$	-1	11.12	899.0	341
T_d-C_{28}	$+1$	8.73	1145.0	129	I_h-C_{60}	-3	18.30	546.3	332
$C_{2v}-II-C_{30}$	$+1$	8.42	1187.7	118	T_d-C_{28}	-4	13.71	729.5	318
D_2-C_{28}	0	8.58	1164.9	102	T_d-C_{28}	-4	7.62	1312.1	271
$C_{2v}-I-C_{30}$	$+1$	11.26	887.9	99	I_h-C_{60}	-2	8.68	1152.2	210
T_d-C_{28}	$+1$	10.14	986.3	96	I_h-C_{60}	-2	18.19	549.8	208
T_d-C_{28}	$+1$	8.33	1200.5	96	T_d-C_{28}	-3	13.56	737.2	207
I_h-C_{60}	$+1$	8.45	1183.8	95	$D_{6d}-C_{24}$	-1	7.96	1255.6	185
$D_{6d}-C_{24}$	0	11.58	863.7	85	$C_{2v}-II-C_{30}$	-4	13.47	742.6	182
$D_{6d}-C_{24}$	$+1$	16.00	624.9	77	$C_{2v}-I-C_{30}$	-4	8.09	1236.4	182
I_h-C_{60}	0	19.01	526.0	77	$D_{3h}-C_{26}$	-1	7.86	1272.5	178
I_h-C_{60}	$+1$	7.80	1282.7	76	T_d-C_{28}	-4	16.70	599.0	173
D_2-C_{28}	0	7.21	1387.5	76	$D_{6d}-C_{24}$	-1	8.48	1178.9	167
T_d-C_{28}	0	8.81	1135.0	70	I_h-C_{60}	-1	8.75	1142.7	143
I_h-C_{20}	0	13.60	735.4	66	D_2-C_{28}	-4	7.61	1313.8	143

fullerenes would be to focus on the 13–16 µm spectral window, which contains very few PAH-related modes and is the range associated with radial carbon motion in fullerene cage paired and triplet pentagons (figure 15). For example, neutral $D_{6d}-C_{24}$ shows an intense and sharp peak around 14.8 µm. Bernard-Salas et al. [54] conducted a survey of fullerene-rich planetary nebulae in the Milky Way and the Magellanic clouds, and reported that SMC 16 shows an asymmetric feature that peaks at 14.5 µm which is currently unexplained. Furthermore, we suggest that a better approach to attributing features in stellar spectra should be to move away from single peak fitting to fitting complete signatures. Notably, our objects display several peaks in the 5–20 µm region with varying intensity ratios which should be fitted together to ensure proper species attribution.

Clearly, this study needs extension to allow further unambiguous peak identification, both to larger fullerenes C_n, $30 < n < 60$, and notably to include hydrogenated species. Hydrogen contamination is seen as artefacts in experimental mass spectrum data, and one study suggested that about half of their observed odd-numbered pure carbon clusters C_{2n-1} had a hydrogen atom [55]. We also suggest that in future it would be useful to update the NASA AMES PAH database [17], a useful resource for IR spectral peak assignment, to include spectra for small cage fullerenes.
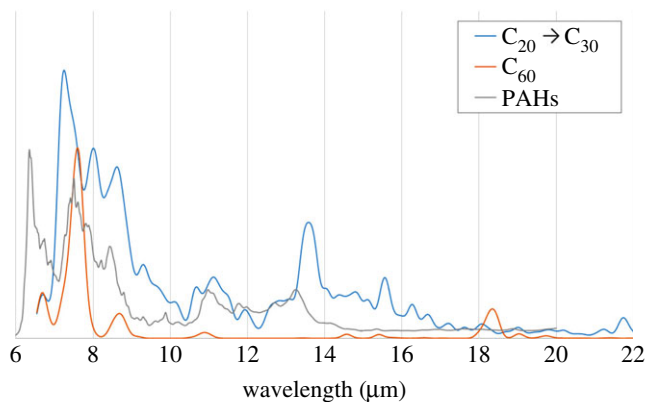
Figure 15. Sum of all 478 purely carbon–hydrogen species in the NASA AMES PAH database. Each spectrum intensity is divided by the number of carbon atoms in the PAH (convolved with a Lorentzian emission profile with a FWHM of 10 cm^{-1}). As can be seen, in good agreement with literature reports of PAH interstellar bands, there is strong absorption across the 6–9 μm range, with secondary features in the 10–14 μm region, and relatively little signal in the 14–20 μm range. In comparison, similarly weighted sums of all small fullerene and C_{60} calculations in this paper notably show extensive fullerene cage modes in the 14–18 μm range.

References

1. Cami J, Bernard-Salas J, Peeters E, Malek SE. 2010 Detection of C_{60} and C_{70} in a young planetary nebula. *Science* **329**, 1180–1182. (doi:10.1126/science.1192035)
2. García-Hernández DA, Manchado A, García-Lario P, Stanghellini L, Villaver E, Shaw RA, Szczerba R, Perea-Calderón JV. 2010 Formation of fullerenes in H-containing planetary nebulae. *Astrophys. J. Lett.* **724**, L39–L43. (doi:10.1088/2041-8205/724/1/L39)
3. García-Hernández DA, Rao NK, Lambert DL. 2011 Are C_{60} molecules detectable in circumstellar shells of R Coronae Borealis stars? *Astrophys. J.* **729**, 126. (doi:10.1088/0004-637X/729/2/126)
4. Gielen C, Cami J, Bouwman J, Peeters E, Min M. 2011 Carbonaceous molecules in the oxygen-rich circumstellar environment of binary post-AGB stars: C_{60} fullerenes and polycyclic aromatic hydrocarbons. *Astron. Astrophys.* **536**, A54. (doi:10.1051/0004-6361/201117961)
5. Sellgren K, Werner MW, Ingalls JG, Smith JDT, Carleton TM, Joblin C. 2010 C_{60} in reflection nebulae. *Astrophys. J. Lett.* **722**, L54–L57. (doi:10.1088/2041-8205/722/1/L54)
6. Zhang Y, Kwok S. 2011 Detection of C_{60} in the protoplanetary nebula IRAS 01005+7910. *Astrophys. J.* **730**, 126. (doi:10.1088/0004-637X/730/2/126)
7. Houck JR *et al.* 2004 The infrared spectrograph (IRS) on the Spitzer space telescope. *Astrophys. J. Suppl. Ser.* **154**, 18–24. (doi:10.1086/423134)

8. Dunk PW, Adjizian J-J, Kaiser NK, Quinn JP, Blakney GT, Ewels CP, Marshall AG, Kroto HW. 2013 Metallofullerene and fullerene formation from condensing carbon gas under conditions of stellar outflows and implication to stardust. *Proc. Natl Acad. Sci. USA* **110**, 18081–18086. (doi:10.1073/pnas.1315928110)

9. Frum CI, Engleman Jr R, Hedderich HG, Bernath PF, Lamb LD, Huffman DR. 1991 The infrared emission spectrum of gas-phase C_{60} (buckmisterfullerene). *Chem. Phys. Lett.* **176**, 504–508. (doi:10.1016/0009-2614(91)90245-5)

10. Nemes L, Ram RS, Bernath PF, Tinker FA, Zumwalt MC, Lamb LD, Huffman DR. 1994 Gas-phase infrared emission spectra of C_{60} and C_{70}. Temperature-dependent studies. *Chem. Phys. Lett.* **218**, 295–303. (doi:10.1016/0009-2614(93)E1488-3)

11. Fulara J, Jakobi M, Maier JP. 1993 Electronic spectra of the C_{70} molecule and C_{70}^+, C_{70}^- ions in neon matrices. *Chem. Phys. Lett.* **206**, 203–209. (doi:10.1016/0009-2614(93)85542-V)

12. Canton SE, Yencha AJ, Kukk E, Bozek JD, Lopes MCA, Snell G, Berrah N. 2002 Experimental evidence of a dynamic Jahn-Teller effect in C_{60}^+. *Phys. Rev. Lett.* **89**, 045502. (doi:10.1103/PhysRevLett.89.045502)

13. Léger A, d'Hendecourt L, Boccara N (eds). 1986 *Polycyclic aromatic hydrocarbons and astrophysics*. Dordrecht, The Netherlands: Springer.

14. Campbell EK, Holz M, Gerlich D, Maier JP. 2015 Laboratory confirmation of C60+ as the carrier of two diffuse interstellar bands. *Nature* **523**, 322–323. (doi:10.1038/nature14566)

15. Foing BH, Ehrenfreund P. 1994 Detection of two interstellar absorption bands coincident with spectral features of C60+. *Nature* **369**, 296–298. (doi:10.1038/369296a0)

16. Shinohara H. 2000 Endohedral metallofullerenes. *Rep. Prog. Phys.* **63**, 843–892. (doi:10.1088/0034-4885/63/6/201)

17. Boersma C *et al*. 2014 The NASA AMES PAH IR spectroscopic database version 2.00: updated content, web site, and on(off)line tools. *Astrophys. J. Suppl. Ser.* **211**, 8. (doi:10.1088/0067-0049/211/1/8)

18. Kroto HW. 1987 The stability of the fullerenes Cn, with $n = 24, 28, 32, 36, 50, 60$ and 70. *Nature* **329**, 529–531. (doi:10.1038/329529a0)

19. O'brien SC, Heath JR, Kroto HW, Curl RF, Smalley RE. 1986 A reply to 'magic numbers in C_n^+ and C_n^- abundance distribution' based on experimental observations. *Chem. Phys. Lett.* **132**, 99–102. (doi:10.1016/0009-2614(86)80703-5)

20. Dunk PW, Kaiser NK, Mulet-Gas M, Rodríguez-Fortea A, Poblet JM, Shinohara H, Hendrickson CL, Marshall AG, Kroto HW. 2012 The smallest stable fullerene, M@C_{28} (M = Ti, Zr, U): stabilization and growth from carbon vapor. *J. Am. Chem. Soc.* **134**, 9380–9389. (doi:10.1021/ja302398h)

21. Yamaguchi Y, Maruyama S. 1999 A molecular dynamics study on the formation of metallofullerene. *Eur. Phys. J. At. Mol. Opt. Plasma Phys.* **9**, 385–388. (doi:10.1007/s100530050462)

22. Dunk PW, Mulet-Gas M, Nakanishi Y, Kaiser NK, Rodríguez-Fortea A, Shinohara H, Poblet JM, Marshall AG, Kroto HW. 2014 Bottom-up formation of endohedral mono-metallofullerenes is directed by charge transfer. *Nat. Commun.* **5**, 5844. (doi:10.1038/ncomms6844)

23. Nagase S, Kobayashi K, Akasaka T. 1998 Recent advances in the structural determination of endohedral metallofullerenes. *J. Comput. Chem.* **19**, 232–239. (doi:10.1002/(SICI)1096-987X(19980130)19:2<232::AID-JCC16>3.0.CO;2-J)

24. Kobayashi K, Nagase S. 1998 Structures and electronic states of M@C_{82} (M = Sc, Y, La and lanthanides). *Chem. Phys. Lett.* **282**, 325–329. (doi:10.1016/S0009-2614(97)01328-6)

25. Lebedkin S, Renker B, Heid R, Schober H, Rietschel H. 1998 A spectroscopic study of M@C_{82} metallofullerenes: Raman, far-infrared, and neutron scattering results. *Appl. Phys. A* **66**, 273–280. (doi:10.1007/s003390050666)

26. Frisch MJ, Trucks GW, Schlegel HB, Scuseria GE, Robb MA. 2009 *Gaussian 09, Revision E.01*. Wallingford, CT: Gaussian Inc.

27. Bauschlicher CW *et al*. 2010 The NASA AMES polycyclic aromatic hydrocarbon infrared spectroscopic database: the computed spectra. *Astrophys. J. Suppl. Ser.* **189**, 341–351. (doi:10.1088/0067-0049/189/2/341)

28. An W, Shao N, Bulusu S, Zeng XC. 2008 Ab initio calculation of carbon clusters. II. Relative stabilities of fullerene and nonfullerene C_{24}. *J. Chem. Phys.* **128**, 084301. (doi:10.1063/1.2831917)

29. An J, Gan L-H, Zhao J-Q, Li R. 2010 A global search for the lowest energy isomer of C_{26}. *J. Chem. Phys.* **132**, 154304. (doi:10.1063/1.3364801)

30. Walker GAH, Bohlender DA, Maier JP, Campbell EK. 2015 Identification of more interstellar C_{60}^+ bands. *Astrophys. J. Lett.* **812**, L8. (doi:10.1088/2041-8205/812/1/L8)

31. Kern B, Strelnikov D, Weis P, Böttcher A, Kappes MM. 2013 IR absorptions of C_{60}^+ and C_{60}^- in neon matrixes. *J. Phys. Chem. A* **117**, 8251–8255. (doi:10.1021/jp4054605)

32. Strelnikov D, Kern B, Kappes MM. 2015 On observing C_{60}^+ and C_{60}^{2+} in laboratory and space. *Astron. Astrophys.* **584**, A55. (doi:10.1051/0004-6361/201527234)

33. Kern B, Strelnikov D, Weis P, Böttcher A, Kappes MM. 2014 IR, NIR, and UV absorption spectroscopy of C_{60}^{2+} and C_{60}^{3+} in neon matrixes. *J. Phys. Chem. Lett.* **5**, 457–460. (doi:10.1021/jz402630z)

34. Krause M, Hulman M, Kuzmany H, Dennis TJS, Inakuma M, Shinohara H. 1999 Diatomic metal encapsulates in fullerene cages: a Raman and infrared analysis of C_{84} and $Sc_2@C_{84}$ with D_{2d} symmetry. *J. Chem. Phys.* **111**, 7976–7984. (doi:10.1063/1.480131)

35. Hulman M, Pichler T, Kuzmany H, Zerbetto F, Yamamoto E, Shinohara HN. 1997 Vibrational structure of C_{84} and $Sc_2@C_{84}$ analyzed by IR spectroscopy. *J. Mol. Struct.* **408–409**, 359–362. (doi:10.1016/S0022-2860(96)09545-2)

36. Prinzbach H, Weiler A, Landenberger P, Wahl F, Wörth J, Scott LT, Gelmont M, Olevano D, Issendorff Bv. 2000 Gas-phase production and photoelectron spectroscopy of the smallest fullerene, C_{20}. *Nature* **407**, 60–63. (doi:10.1038/35024037)

37. Paulus B. 2003 Electronic and structural properties of the cage-like molecules C_{20} to C_{36}. *Phys. Chem. Chem. Phys.* **5**, 3364–3367. (doi:10.1039/B304539K)

38. Zamani M, Motahari A, Dabbagh HA, Farrokhpour H. 2014 IR and UV spectroscopic analysis of C_{20} carbon nanostructures. *NanoAnalysis* **1**, 31–40.

39. Wu J, Sun Z, Li X, Ma B, Tian M, Li S. 2011 Theoretical study on the smallest endohedral metallofullerenes: $TM@C_{20}$ (TM = Ce and Gd). *Int. J. Quantum Chem.* **111**, 3786–3792. (doi:10.1002/qua.22908)

40. Kent PRC, Towler MD, Needs RJ, Rajagopal G. 2000 Carbon clusters near the crossover to fullerene stability. *Phys. Rev. B* **62**, 15 394–15 397. (doi:10.1103/PhysRevB.62.15394)

41. Martin JML, El-Yazal J, François J-P. 1996 On the structure and vibrational frequencies of C_{24}. *Chem. Phys. Lett.* **255**, 7–14. (doi:10.1016/0009-2614(96)00347-8)

42. Cox DM, Trevor DJ, Reichmann KC, Kaldor A. 1986 C_{60}La: a deflated soccer ball? *J. Am. Chem. Soc.* **108**, 2457–2458. (doi:10.1021/ja00269a060)

43. Sheng X-L, Yan Q-B, Zheng Q-R, Su G. 2009 Boron fullerenes B32+8 k with four-membered rings and B32 solid phases: geometrical structures and electronic properties. *Phys. Chem. Chem. Phys.* **11**, 9696–9702. (doi:10.1039/B911519F)

44. Guo T, Smalley RE, Scuseria GE. 1993 Ab initio theoretical predictions of C_{28}, $C_{28}H_4$, $C_{28}F_4$, $(Ti@C_{28})H_4$, and $M@C_{28}$ (M = Mg, Al, Si, S, Ca, Sc, Ti, Ge, Zr, and Sn). *J. Chem. Phys.* **99**, 352–359. (doi:10.1063/1.465758)

45. Guo T *et al.* 1992 Uranium stabilization of C_{28}: a tetravalent fullerene. *Science* **257**, 1661–1664. (doi:10.1126/science.257.5077.1661)

46. Shelimov KB, Clemmer DE, Jarrold MF. 1995 Structures and isomerization of LaC_n^+ clusters. *J. Phys. Chem.* **99**, 11 376–11 386. (doi:10.1021/j100029a013)

47. Nishikawa O, Taniguchi M, Saito Y. 2008 Study of characteristic fragmentation of nanocarbon by the scanning atom probe. *J. Vac. Sci. Technol. A* **26**, 1074–1078. (doi:10.1116/1.2832364)

48. Skwara B, Góra RW, Zaleśny R, Lipkowski P, Bartkowiak W, Reis H, Papadopoulos MG, Luis JM, Kirtman B. 2011 Electronic structure, bonding, spectra, and linear and nonlinear electric properties of $Ti@C_{28}$. *J. Phys. Chem. A* **115**, 10 370–10 381. (doi:10.1021/jp206331n)

49. García-Hernández DA, Iglesias-Groth S, Acosta-Pulido JA, Manchado A, García-Lario P, Stanghellini L, Villaver E, Shaw RA, Cataldo F. 2011 The formation of fullerenes: clues from new C_{60}, C_{70}, and (possible) planar C_{24} detections in magellanic cloud planetary nebulae. *Astrophys. J. Lett.* **737**, L30. (doi:10.1088/2041-8205/737/2/L30)

50. Geballe TR, Tielens AGGM, Allamandola LJ, Moorhouse A, Brand PWJL. 1989 Spatial variations of the 3 micron emission features within UV-excited nebulae—photochemical evolution of interstellar polycyclic aromatic hydrocarbons. *Astrophys. J.* **341**, 278. (doi:10.1086/167491)

51. Cohen M, Tielens AGGM, Bregman J, Witteborn FC, Rank DM, Allamandola LJ, Wooden D, Jourdain de Muizon M. 1989 The infrared emission bands. III—Southern IRAS sources. *Astrophys. J.* **341**, 246. (doi:10.1086/167489)
52. Gilette FC, Forest WJ. 1973 Spectra of the Becklin-Beugebauer point source and the Kleinmann-Low nebula from 2.8-13.5 microns. *Astrophys. J.* **179**, 483–491. (doi:10.1086/151888)
53. Boersma C, Bauschlicher CW, Allamandola LJ, Ricca A, Peeters E, Tielens AGGM. 2010 The 15–20 μm PAH emission features: probes of individual PAHs? *Astron. Astrophys.* **511**, A32. (doi:10.1051/0004-6361/200912714)
54. Bernard-Salas J, Cami J, Peeters E, Jones AP, Micelotta ER, Groenewegen MAT. 2012 On the excitation and formation of circumstellar fullerenes. *Astrophys. J.* **757**, 41. (doi:10.1088/0004-637X/757/1/41)
55. Maruyama S, Kohno M, Inoue S. 2000 Chemical reaction of metal-carbon binary cluster anions by FT-ICR mass spectrometer. In *Mass Spectrometer, fullerene 2000: chemistry and physics of fullerenes and carbon nanomaterials*, vol. 10 (eds PV Kamat, DM Guldi, KM Kadish), pp. 309–319. Pennington, NJ: The Electrochemical Society.